Acoustic measurement and morphological features of organic sediment deposits in combined sewer networks

Iacopo Carnacina[1], *Frédérique Larrarte*[2], *Nicoletta Leonardi*[3]

[1]AIR Worldwide Ltd, 40 Gracechurch St, London, EC3V 0BT, UK Tel: +44 020 3764 0300

[2]LUNAM Université, IFSTTAR, GER, F-44341 Bouguenais, France. Tel: +33 (0)2 40 84 58 00 Fax : +33 (0)2 40 84 59 99

[3]University of Liverpool, Department of Geography and Planning, Roxby Building, 74 Bedford St S, Liverpool L69 7ZT, UK

ABSTRACT

The performance of sewer networks has important consequences from an environmental and social point of view. Poor functioning can result in flood risk and pollution at a large scale.

Sediment deposits forming in sewer trunks might severely compromise the sewer line by affecting the flow field, reducing cross-sectional areas, and increasing roughness coefficients.

In spite of numerous efforts, the morphological features of these depositional environments remain poorly understood. The interface between water and sediment remains inefficiently identified and the estimation of the stock of deposit is frequently inaccurate. In part, this is due to technical issues connected to difficulties in collecting accurate field measurements without disrupting existing morphologies. In this paper, results from an extensive field campaign are presented; during the campaign a new survey methodology based on acoustic techniques has been tested. Furthermore, a new algorithm for the detection of the soil-water interface, and therefore for the correct esteem of sediment stocks is proposed. Finally, results in regard to bed topography, and morphological features at two different field sites are presented and reveal that a large variability in bed forms is present along sewer networks.

Keywords: sonar profiler, morphology, organic sediment, sewer deposits

1. INTRODUCTION

Sewer networks are essential for urban areas and their performance has important environmental consequences because it determines the quality of sanitation, and influence the risk of urban flooding (e.g. European standard NF EN 14654-1). Standard norms for environmental impact of sanitation facilities establish that sedimentation in sewer trunks should be prevented in order to avoid both flooding, and pollution issues. In fact, sediment accumulations have two main consequences: firstly, they reduce the ability to evacuate wastewater due to changes in friction and in cross sectional area; secondly, due to their organic nature, these sediments can be easily eroded and contaminate nearby areas. In spite of these deleterious effects, sediment deposits generally occur and interest large parts of sewer trunks; therefore, is important to understand their properties, and to identify effective methodologies aimed at characterizing their morphological features.

Difficulties arise when trying to study these depositional environments due to health and safety, as well as technical issues. Classically, sediment accumulations were detected using mechanical probes, i.e., point gauges, optical backscatter probes or endoscopes (Oms 2003). The limitations of these methodologies are connected to the fact that the sediment interface might be strongly perturbed leading to a misevaluation of the amount of sediments, especially in the presence of very soft fractions. Limitations are also caused by the fact that these instruments frequently necessitate the installation of large and unpractical equipment (Ahyerre et al. 2001). Moreover, these sensors are mostly punctual and difficult to use to trace fine resolution transverse profiles of the sewer trunks. More recently, Bertrand-Krajewski and Gibello, 2008 proposed the use of ultrasonic methodology to investigate the sediment bottom, and by using a rotating device showed that this technology could be potentially used inside sewer networks. However, no information about the nature of the sediment deposits was given, and preliminary results were only based probe outputs. (Gourmelen et al. 2010) also developed an acoustic system and provided new insights about

sediment interface trough continuous observations; however observations were in part limited by their punctuality.

Within this context, this manuscript has a dual goal: first, a new technique, and procedure for the analysis of sediment deposits, and more accurate identification of the soft sediment interface is presented; the technique is based on an acoustic technology and a rotating sonar head. In this regard a new algorithm for a more accurate identification of the interface boundary is also defined. Measurements are then compared with results obtained with classical sediment gauges and sediment sampler.

Secondly, by using the aforementioned methodology, and fast Fourier analysis, new insights about the bathymetry, and morphology of combined sewer network bed forms are provided for two sewers in the city of Nantes (France).

2 LITTERATURE REVIEW

Characteristics of sediment interface

Combined sewer networks are characterized by a significant variability in sediment types and sediment transport patterns. (Crabtree 1989) classified sediment deposits based on the characteristics of their fractions; among those individuated by the Author, the two of interest for the present study are: Type A deposits: coarse, granular bed material-widespread; Type C deposit: mobile, fine grained found in slack zones in isolation and overlaying Type A. Type C deposits are characterised by larger fraction of organic material and a weak shear resistance.

During dry weather, a weak layer (type C) with organic content >90%, and of d_{50} around 0.5 mm is generally observed above a coarser type A layer. This weak layer is easily re-entrained when the shear stress is higher than 0.5-1 N/m^2.

Observation by (Oms 2003) confirm this multiple layers structure. According to endoscope measurements, coarser deposits are present at the bottom, and are covered by a layer of fine organic

material having bulk density ρ_b in between 1046 kg/m^3 and 1315 kg/m^3. Herein, sediment interface is defined as the exterior boundary of the weak (type C) sediment layer.

(Ashley et al. 2004) further introduced two different definitions based on sampling technique, namely, near bed solids and dense undercurrent. In fact, apart from sediments in suspension, transport patterns are generally characterized by a combination of bed load over the settled bed and an inner suspension. The near bed organic solids which are transported over the settled bed, are generally detected trough sediment traps, and for dry weather flow are characterised by an organic content greater than 90% and sediment diameters d_{50} ranging from 30 mm to 50 mm. The inner suspension can be detected when sediments are collected with pipes, in form of a dense undercurrent, characterised by particles which are not in contact with the bed and which have a large dimension compared to that in the main flow field.

(Arthur et al. 1996) studied the characteristics of what has been defined as "organic near bed transport" in the Dundee combined sewage system. In this case, organic near bed fluid sediments were characterised by large volatile contents (up to 87.6%), small median radius d_{50} as 0.09mm<d_{50}<11 mm and bulk density ρ_b from 1000 kg/m^3 to 1998 kg/m^3.

Observation in the combined sewer system of Paris (Ahyerre et al. 2001), both visual and with suction systems, revealed the existence of high concentrated layer (total suspended solid concentrations up to 2 g/l) within the water column, in correspondence with what has been considered the organic layer. However, visual observation of the sediment water interface suggests that high concentrations might be linked to the survey methodology rather than to the presence of fluid sediment. In fact, direct observation during dry weather confirmed a clear distinction between water and organic layer, with only few particles moving on the top of the interface.

Laplace et al., 2003 showed that the deposits in sewers, and especially the organic layer at the water interface contribute to 40 to 70% of the total pollution from the wet weather combined sewer flow, and suggest that the organic layer formed at the surface of the deposit could be thus washed off trough flushing techniques before rainstorms. Gasperi et al., 2010 highlighted the significant role of

105 sewer sediments as a source of Wet Weather Flow pollution, and suggested the possible importance
106 of preventive managing service sewer actions to reduce the pollutant stocks. By using an extensive
107 database of flow and turbidity measurements from Paris and Lyon, Hannouche et al., 2014
108 confirmed that the contribution of sewer depots to wet weather suspended solid discharge is
109 important and up to 80%. By using laboratory experiments, it has been also shown that the
110 stratification of the sediment bed can originate from biological mechanisms. Specifically, surface
111 layers are influenced by environmental conditions and oxygen levels. A significantly weaker
112 sediment layer with lower shear strength values is formed under more quiescent and oxygen richer
113 conditions (Banasiak et al., 2005). Weather conditions are important for the characteristics of
114 sediment deposits as well. Bersinger et al., 2015 showed that the sediment deposit is renewed after
115 each rainfall event because, as the flow in pipes slows down, there is an accumulation of new
116 sediments in the sewer. However, sedimentation processes are not the sole reason for stock
117 renewal, and the authors suggest that the sewer network behaves as a bio-physicochemical reactor,
118 and that biological processes leads to in-sewer transformation of deposits. Bersinger et al., 2015,
119 also suggest that sediment stocks in sewer network during dry weather periods might be calculated
120 by estimating the daily chemical oxygen demand fluxes brought about by the different rainfall
121 events of the month.
122 In spite of numerous and valuable studies, there are still many uncertainties connected to grain size
123 distribution, morphological features, as well as about the exact location of sediment interfaces.
124 Many times, these uncertainties are connected to sampling techniques which are too invasive and
125 disrupt the flow field.
126
127 ***Detection of the sediment deposit interface***
128 Different techniques have been employed to identify the sediment-water interface, but many times
129 environmental and security constraints are present.

130 Development of optical and acoustical backscatter probes for marine applications allow the
131 definition of sediment bottoms trough indirect measurements. For example, (Gallagher et al. 1996)
132 defined the distance at which the seafloor was detected using a threshold criterion, and by means of
133 1 MHz sonar altimeter with voltage immediately below the automatic adjusted maximum gain
134 level. After laboratory and field experiences, they defined an automatic gain adjustment algorithm,
135 which included signal normalization and a threshold voltage employed to individuate the time at
136 which the bottom-echo was detected. By means of the automatic gain adjustment algorithm, the
137 authors were able to measure the seafloor with a precision of 0.03 m. Differently, (Bell and Thorne
138 1997), located the sediment bottom on the base of the maximum correlation calculated between the
139 backscatter profile measured with a 2 MHz rotating head sonar and a model bed echo which
140 reflects an ideal approximation of what is the actual bed echo.
141 According to (Bell and Thorne 1997) and (Thorne and Hanes 2002) the use of the algorithm
142 improves the localisation of the sediment bottom if compared to threshold methodologies.
143 Moreover, the authors provide a full review of acoustic measurements technique and methodologies
144 to determine the sediment concentration from the backscatter profile.
145 (Webb and Vincent 1999), based on three frequency transducer experiments, defined the bed as the
146 place where the strongest backscatter signal is measured.
147 Later on, (Green and Black 1999) define the base range as the range of the bin (i.e. one of the
148 volumes in which the water column is divided in the sonar image) immediately above the break of
149 slope in the temporal burst-averaged concentration profile. The burst-average concentration profile
150 was based on the averaged root-mean-square backscattered pressure profiles. According to the
151 nature of the surveyed bed, they namely located the sediment bottom at 0.01 m below the base
152 range for rippled bed, and at 0.02 cm below the base range for transitional and “hummocky” beds
153 (i.e., a stratification in which mounds of sand occur).
154 (Hoitink and Hoekstra 2005), compared the suspend concentration profiles obtained from acoustic
155 Doppler current profiler (ADCP), acoustic backscatter signal and optical backscatter signal (OBS).

156 By also considering (Alexander et al. 1997) results, they observed that acoustic instruments have
157 different degree of penetration inside fluid mud according to the signal frequency at which the
158 backscatter is collected. Generally, 200 kHz signal is able to detect the top of the mud layer,
159 corresponding to roughly 1050 kg/m^3, but the reflected signal is more properly associated to a
160 gradient of concentration rather than to a specific density. Differently, lower signal of 20-40 kHz
161 are able to penetrate the fluid mud reaching a more consolidated layer.
162 However, in terms of dredging volume definitions, none of the previous elevations seemed suitable
163 and a more appropriate layer definition comes from intrusive instrumentations, such as sled
164 transducer, which has been designed to travel along a physical horizon of constant density and
165 viscosity (Alexander et al. 1997). More recently, (Dolphin and Vincent 2009), adopted the
166 methodology proposed by (Green and Black 1999) and locate the sediment bottom as the level at
167 which the "break-in-slope" of the sediment concentration curve was observed from acoustic
168 backscatter measurements.
169 It is worth noticing that the majority of technical advancements in terms of acoustic
170 instrumentations have been done in relation to marine environments, where sandy deposits are
171 abundant. Sewer deposits are dramatically different with respect to marine sediments, as they have
172 a much higher organic matter concentration (30% to 89% of volatile solids), and are less
173 homogeneous. Acoustic measurement may represent an adequate solution in terms of installation
174 feasibility (small dimensions and light < 5 kg, no needs of special equipment, and the ability to
175 detect the interface with minimal interaction, a characteristic rather important in presence of soft
176 sediments.
177

178 **3 METHODS**

179 **Equipment**

180 Herein, a sonar profiler is used to detect the interface of the sediment deposits, and then compare
181 the acoustic measurements with data from a sediment gauge. Water samples were collected as well.

182 The use of a sonar profiler in sewer network is a relatively unexplored technology. Results from the
183 sonar were improved by modifying the algorithm used to extract the sediment interface. In this
184 regard, a sonar profiler (thereafter mentioned SONAR), manufactured by Marine Electronics ltd.,
185 and with 2 MHz working frequency was used to measure the bottom transverse and longitudinal
186 acoustic response of the sediment bed.
187 The profiler consisted in an emitter and an acoustic receiver that rotates inside the probe case. The
188 probe case consisted of an alloy cylinder of 70 mm of diameter and 445 mm of length. The sonar
189 profiler has a rotating head that measure the acoustic backscatter along 400 beams of 0.9° each and
190 for 250 control volumes, or bin, from the centre of the probe to the maximal measured distance or
191 range R_{max}, with a frequency of 1 Hz (i.e., a section each second).
192 The plane of rotation is located at around 4.5 cm from the edge of the PVC boot. The probe can
193 detect the acoustic backscatter (ABS) with maximum distances (subscript "max") ranging between
194 0.125 m < R_{max} < 6 m, where R is the generic position of the control volume or bin from the
195 SONAR centre (Figure 1c). The probe is able to detect both pitch and roll angles (right bottom of
196 the frame), with a precision of ±0.1°. The main parameters to regulate were:
197 1) the "range" or maximum detectable distance, R_{max} (0.125 < R_{max} < 6 m); Since each radial beam
198 is divided into 250 control volume between $0<R<R_{max}$, the probe presents a geometrical resolution
199 of 1/250 of the maximum range.
200 2) the "pulse length", P_L (4 μs <P_L<20 μs), which represent the duration of the pulse generated by
201 the sonar; the vertical resolution δ_v is connected to P_L by $\delta_v=cP_L/2$.
202 The output generated by the software is given in counts using an 8-bit scale. The SONAR is
203 equipped with a 70 dB logarithmic receiver, in which the output voltage (the voltage post-processed
204 by the probe and which is latter converted in counts) produced by the probe is proportional to the
205 logarithm of the input voltage (i.e., the row signal recorded by the piezoelectric transducer of the
206 SONAR). The software automatically adjusts the gain to the largest detected backscatter. However,
207 the output also gives the gain used for the automatic adjustment.

208 The software also allows for the regulation of the maximal intensity and the signal threshold,
209 which, however, does not modify the accuracy of the measure. The temperature needs to be
210 manually adjusted, as the probe has not been equipped with a thermometer. Hence, temperatures
211 have been recorded by means of a digital thermometer installed in the network, with precision of
212 0.1°C and regularly calibrated.
213 The software elaborates separately each beam or sector of 0.9°. A profile of the bottom can be
214 obtained by the recorded image using three different software algorithms: 1) "Max", the profile is
215 obtained from the points were the maximum ABS is detected; 2) "3/4", the profile is obtained from
216 the point were ¾ of the maximum ABS is detected; 3) "Area1", the profile is obtained from the
217 point were the largest energy is detected. Generally, "Max" shows a profile that is more extended
218 compared to the other two. Slight differences occurs between them, generally less than 1 cm over
219 hard bottom, while the profile individuated over soft deposits is more scattered.
220 In terms of sediment gauge measurements, when soft sediments (e.g. the type C organic layer) are
221 present, the introduction of the gauge might interfere with the sediments and destroys the organic
222 layer. To limit this issue, a point sediment gauge fixed at the bottom and with 25 cm disk diameter
223 was used. When operating with a sediment gauge, the ability of the operator to detect the sediment
224 represents a source of uncertainty as well. In this regard, to reach the top of the organic layer
225 without entering it, the gauge should be introduced without any pressure on the disc. Water has
226 been sampled using a suspended solid sampler device, made of four pipes of 10 mm of diameter,
227 placed at different heights from the bottom (Jaumouillie et al. 2002). Each pipe is connected to a
228 2.5 l bottle with -0.07 MPa pressure. Once the pipes were connected to the bottles, the device was
229 immersed, and the connectors opened for around 15 second.
230 **Field sites**
231 The "Duchesse Anne" combined sewer (DA) and the "Allée de l'Erdre" combined sewer (AE)
232 were chosen based on their different flow characteristics as well as differences in bottom and
233 suspended sediment concentrations

234 The DA site is characterised by a slope of S=0.3% (%), a catchments area of 4.11km^2, connected
235 into a network of 21 km of length. The AE site has a slope of S=1.2 %, a catchments area of 1.41
236 km^2 ha and a network length of about 60 km. Table 1 summarizes flow characteristics, and
237 sediment deposits characteristics for the two different sites and during the execution of the field
238 campaign. Flow velocity at the DA site are, on average, 4 times higher than flow velocities at site
239 AE, while the sediment stack at the AE site is on average 5 times higher than at the DA site (Table
240 1). All tests were executed in the absence of precipitation, and apart from test AE-S2 all tests were
241 conducted after at least two days of dry weather (<0.2 mm precipitation, T_D Table 1). The number
242 of dry weather days before the tests ranged from 0 to 10. During dry weather, the DA sewer
243 sediment deposits have a mineral content (type A sediment, according to (Crabtree 1989)) higher
244 than AE. The AE site generally shows, starting from the bottom, a first layer of type A sediments, a
245 second layer of type C, and superimposed layer with high suspended sediments. Figure 1f presents
246 an example, of sediment layering.
247 Both sewer pipes are characterised by an egg shaped transverse section with one lateral bank,
248 allowing the passage of the operators, and preventing sediment disturbance (Figure 1 a,b).
249 Two different carriage systems have been installed inside the sewer in order to shift the probes both
250 longitudinally and transversally. At the AE site, two rails have been installed longitudinally at the
251 invert sides toward 10 m of length at about 1.2 m from the invert bottom, in order to reduce their
252 inundation likelihood and the flow disturbance. The rails have been fixed starting from the manhole
253 toward the upstream direction (Figure 1d), and consisted of 4 cm width squared alloy bars. A 1.08
254 m alloy bar of the same dimensions and section of that used for the rail has been fixed transversally
255 over the rails and a mobile support, which can slide along all the channel width, held the vertical
256 bars. In order to adjust the probe orientation, the vertical bar consisted of a cylindrical section that
257 completely rotates in both directions. Differently, the experimental installation of DA site (Figure
258 1e) consisted of a single rail fixed at the top of the invert, over which a carriage has been arranged,
259 allowing for longitudinal movements. Vertically, the position of the probes is regulated by means

of a cylindrical bar, directly hanging from the small carriage, which again can be rotated in order to adjust the probe orientation. Small transverse regulations are possible to fix the probe at the dry weather channel centre. The longitudinal position of the probe is measured by means of a 1 cm precise scale fixed over the rail. A transverse bar has been used to stabilize the whole system, hence preventing and reducing lateral probe oscillations and tilting.

Measurements executions

Data presented here refer to sewer trunks in the DA-field site, and in the AE-field sites (trunks length ranging from 4 to 9km). For each transverse section, the probe centre has been fixed at the free surface over the invert centre, in order to minimize flow disturbance. For each sampled section, a SONAR image is recorded and the sewer profile extracted, with a resolution between 10 cm and 20 cm longitudinally. The image is thus made by the backscatter intensity detected at each sector of 0.9 rad. In real time conditions and based on the 8-bit backscatter intensity, the SONAR software shows the bottom profile using the max algorithms by considering the line connecting the point at which the maximum backscatter intensity is detected for each sector (Figure 2). The extensive measurement campaign was made between October 2010 and June 2011, generally between 7:30 am and 11:00 am, when the flow level was low enough to reduce the risk for the operators.

RESULTS

The algorithms developed by Marine Electronics shows a good correspondence with the observed geometry in laboratory conditions (Figure 2a) and, more in general with compacted material (concrete, sand,) as represented by white continuous lines representing the sewer contour (Figure 2a, b). However, these algorithms fail to detect the exact interface of the soft deposits (Figure 2b, the solid interface detected by the Marine Electronics algorithm is the red dashed line). Using a similar approach as (Green and Black 1999), a new algorithm has been defined which identifies the

acoustic interface as the distance from the probe where the backscatter signal showed the largest gradient.

To reduce possible noise, and before gradient calculation, a Gaussian filter with 5 mm variance (equal to the instrumental variance) and of 10 cell extension was also applied for each beam (equation 1).

$$f'(R) = f * g(R) = \int_{r=0}^{r=R} f(R) \cdot g(\varsigma - R) dR \quad (1)$$

This digital filtration aims at removing, from the original signal, spikes and noise possibly provoking a false detection. The interface is, thus calculated using eq. 2:

$$R_{\text{int}}{}^{j} = \max\left[f'(R^{j}) \right] \text{ for } 0<j<400 \quad (2)$$

in which j represents the j^{th} beam of 0.9° detected by the SONAR. In this regard, an automated script has been developed.

Figure 2c shows an example of the application of eq. 1, 2 to the row signal (square symbols) for the detection of the interface. The original algorithm associate the solid interface to the value R=310 mm where the signal itself reaches the maximum. Differently, the new algorithm associates the solid interface to the maximum of the filtered signal gradient (continuous line), and consequently to *R*=255 mm (Figure 2c).

Figure 3a, b show filtration results, and the final soil interface detection. The sonar image blurs after the application of the filter (compare figure 3a and 3b), but also remove some noise and high spikes from the original source signal, which is advantageous to detect the interface. The final soil interface is indicated by the white circles in figure 3b (note that the number of circles in the figure has been reduced for readability), and is in better agreement with the image itself.

The profile obtained still contains some scatter, due to the presence of large cluster of debris flowing in the water. The automated script generated for this procedure also filters the scatter obtained by the previous procedure. The filter is based on both manual and automated procedure. The manual procedure allows the user to select the points to be eliminated using a rectangular box

selection. The points included in the rectangular selection will be eliminated from the section. The automated procedure is based on a mobile median and standard deviation obtained from the z_{i-5} and z_{i+5} data, where z_i is the i-th point of the vertical component of the interface. Hence, the space of acceptable values is defined as the median value ± median absolute deviation obtained using a windows size of 7 points. Herein, the size of the windows has been used to better capture local patterns (Menold et al. 1999). If the value of z_i is outside the threshold is rejected, otherwise is retained. This procedure is done for all the points of the profile detected by the sonar. The algorithm is repeated until the differences between the n-step standard deviation and the n-1-step is zero.

Figure 3c shows the reconstructed morphology for one of the trunks, and by using the abovementioned methodologies. The black dots in the figure represent the row data after filtration, while the surface represents the interpolated surface using a least square interpolation algorithm.

Tests have been also conducted to verify the accuracy of the SONAR methodology with respect to gauge measurements. One of the test has been carried out at the DA site (section S1), were sediment characteristics were relatively constant (high mineral content). The SONAR rotating head has been stream wise oriented to measure a transverse profile of the sewer trunk (Figure 1d). Figure 4a shows the backscatter contour lines obtained from the SONAR image. Signal of less than 20 counts has been removed from the image, in order to increase the contrast between the water and the deposits. The image has been obtained with a pulse length of 4 μs and a range of 750 mm. According to the 8-bit backscatter amplitude, high backscatter signal corresponds to high amplitude recorded by the SONAR. The image clearly shows the lateral walls of the trunk, of which one is the vertical wall of the side bank. From this image it has been possible to obtain a 8-bit backscattered vertical profile from the centre of the probe (Figure 4b). In the plot, the range has been fixed from the centre of the probe. The centre of the probe relates to the probe dead zone, which is automatically filtered by the software and automatically set to 0 counts of amplitude. The first peak observed at about 15 cm from the centre related to a noise detected by the probe and not filtered.

For -0.15 m $< z_{SONAR} <$ -0.35 m, the backscatter shows an almost constant value of about 20 counts. When the signal approaches the sediment bottom, the signal amplitude drops to about 181 counts and then reduces due to the presence of the sediment on the bottom. The signal shows a marked peak where the sediments have been detected by the gauge. The image shows that the sediment bottom is not perfectly flat, most likely connected to secondary current which could modify the shear stress and the sediment accumulation. In particular, it seems that the larger deposits are present near the left sidewall, whereas less sediment seems to accumulate at the bank wall, owing to larger velocity generally observed in this area for compound section as observed by (Larrarte 2006). According to gauge measurement, an average $z_{SED} = 0.10$ m of sediment has been detected, for a total water depth of δ=0.41 m. SONAR measurement shows a δ_{SONAR}= 0.44 m and a distance between the average sediment plane and the top of the bank of about 0.32 m. The total bank wall height was 0.45 m, therefore showing a sediment depth detected with the sonar of z_{BED}= 0.12 m. A comparison with the value detected with the gauge revealed a reasonable agreement. A slight difference of the order of 20% occurred, which is a satisfactory result. Inaccuracies may occur during gauging operations (the gauge may not reach the bottom, it can slightly sink in the sediment, the sediment morphology is not constant).

5.1 sediment deposits and their morphology

Figure 5a-d shows results obtained from the samples collected at the two different sites. The figure shows both the sediment concentrations in terms of TSS (total suspended solid) and VSS (volatile suspended solids) for two different sieve sizes (0.125 mm and 2 mm) and the bottom particle size distribution, in which D is the diameter for which the percent P in weight of sediment is finer. Figure 5 e-h shows the ratio between VSS and TSS at different water elevations, and for the same tests. TSS, VSS and particle size distribution were determined according to the procedure suggested in French norms: NF EN 872 and NF T 90-105-2, and water samples were collected according to (Larrarte 2008). Standard deviation values for each data point were less than 10 mg/l;

362 this is in agreement with accuracy values presented with the same technique by Larrarte and Pons,
363 2011, and Larrarte, 2015. This technique allows collecting samples of water at different levels from
364 the free surface, and at the same time. The particle size distribution has been evaluated manually
365 for fractions D>0.560 mm and by a MALVERN MS 2000 laser granulometer for fractions D<0.560
366 mm.
367 Bottom sediments show average diameter of about d_{50}=0.1 mm at DA, whilst AE generally shows a
368 smaller diameter of d_{50}=0.025 mm and a sediment uniformity parameter of $\sigma_s=(d_{84}/d_{16})^{0.5}$ of $\sigma_s\approx1.41$
369 and $\sigma_s\approx6$ respectively, i.e., the bottom sediment particle size distribution for DA is rather uniform
370 compared to AE conditions. The difference in the average particle sizes is linked to the averaged
371 velocities observed at the two sites, as shown in table 1. Velocities have been recorder using an
372 acoustic Nivus® PVM-PD of 1 cm/s of precision. The instrument provides averaged velocity but
373 no information about the velocity fluctuation is available. However, three independent
374 measurements have been taken per each survey point, to check their quality and to avoid any
375 influence from suspended material clogging the probe. The standard deviation σ_u has been reported
376 in the table, together with the temperature measurements, necessary to both calibrate the probe and
377 characterise the biological activity of the network. This latter is important as it can deeply modify
378 the characteristics of the surface of the invert and its roughness, e.g., presence of bio-film. Velocity
379 around u=0.4 cm/s occurred at the DA site, in which the sediment thickness was limited to few
380 centimetres. Conversely, AE shows velocities slightly below 10 cm/s during the morning, with
381 sediment deposits thickness larger compared to that observed at DA. Long survey lasting for more
382 than 12 hours shows that generally, later in the morning, the flow velocity increases, while the
383 deposit thickness may considerably reduce. It is worth noticing that a slight change in flow velocity
384 is sufficient to erode the soft deposits.
385 The two sites are also characterised by different concentrations and bottom sediment particle
386 distributions. Both sites are characterised by a large percent of organic matter, as the suspended
387 solids are composed by a volatile fraction generally larger than 70%. However, what clearly

388 distinguish the two sites are the sediment concentrations observed in both the water column and
389 near the bottom (Figure 5). TSS concentrations generally show almost constant values at the DA
390 site of $TSS_{<2mm}$ of 200 mg/l<TSS<350 mg/l, with a slight scatter toward the average observed for
391 each survey. Differently, the AE site shows a strong concentration gradient, with $TSS_{<2mm}$ > 1000
392 mg/l and peaks larger than $TSS_{<2mm}$ > 3000 mg/l, clearly indicating the presence of a mudflow
393 toward the bottom. (Larrarte 2008) also obtained similar results, in which maximum concentration
394 of TSS<600 mg/l and reduced gradients were observed for inverts with few sediment deposits.
395 A sample of sediment deposits typically observed the AE site was presented in Figure 1f.
396 According to field observations, the interface may settle of about 10 cm during the first minute after
397 sampling, demonstrating the presence the rather soft, non-compact type C deposit, easily eroded by
398 slight change in flow velocity (Ashley et al. 1992) and easily suspended during surveys with
399 invasive instrumentation.
400
401 Figure 6 shows results for 4 morphological surveys, one from the DA site and 3 from the AE: DA-
402 S5, AE-S6, AE-S7, and AE-S8 respectively. Each panel represents the morphology of sediment
403 deposits over a length, x, of several km, and over entire cross sections. In the figure, data are
404 displayed in terms of z_{plane}, i.e., the vertical coordinate measured from the average plane passing
405 trough the measured points. An almost bi-dimensional shape characterizes the survey of DA site.
406 Two depression are clearly visible at around x=-1.5 m and x=-7 m, in which observed maximum
407 negative z_{plane} = -40 mm. the central zone of the survey, however, is rather flat and characterized by
408 a maximum deviation of about z_{plane} =40 mm near x=-5.8m.
409 Differently, for the AE sites, the presence of a much higher organic content (Figure 5) alters the
410 previous bi-dimensional patterns observed in case in the DA field site. Test AE-S6 presented a
411 large depressions near x=-500 mm. A similar pattern occurs near x=-1000 mm for AE-S7.
412 The average plane representing the morphology, $z_{average}$, has been further decomposed as $z_{average}$
413 $=\alpha+\beta x+\gamma y$, where α, β, and γ are the minimum squared error coefficients evaluated on the points

414 z_{BED} obtained from the SONAR output. It follows that $z_{plane} = z_{BED}$-$z_{average}$. The horizontal resolution
415 of the survey has been fixed in about 20 cm. Table 2 summarizes coefficients α, β, and γ relative of
416 each survey. Coefficients α represent the thickness of the sediment at the point x=0 m and y=0 and
417 β and γ represent the local longitudinal and transverse slopes respectively. The coefficients of the
418 two sites clearly show large differences.
419 Longitudinal slope coefficients also highlight how sediment deposits may locally presents larger
420 bottom slopes compared to the average invert slope. In particular, DA data shows β of the same
421 order of the bottom invert, due to the low sediment accumulation observed during the survey.
422 Differently, AE presented average slope up to several times larger compared to the bottom slope,
423 where negative beta values correspond to a sediment height decreasing from upstream to
424 downstream. Transverse slope are generally larger than 0.01 for both the sites, indicating the
425 presence of local tridimensional flow patterns. Maximum average transverse may reach up to 7-8%
426 in both sites, regardless the nature of the sediment flow. It is worth noticing that major three-
427 dimensional patterns may be locally generated by the presence of bends and other discontinuities,
428 although these latter are generally more than 10 m upstream the site of measurements.
429 Generally, complicated 3D morphologies have been identified, especially for the AE field sites.
430 Maximum deviations from the average plane may reach larger values, up to z_{plane} =-60 (Figure 6c
431 x=-1000 mm) mm and z_{plane} =+80 mm (Figure 6c x=-2000 mm).
432 These complicated three-dimensional features are characterized by the occurrence of bed forms as
433 well. According to (El Kheiashy et al. 2000; Rauen et al. 2008) bed forms formation are
434 characterized by two main features, i.e., length λ and height η. (Raudkivi 1997; Rauen et al. 2008)
435 proposed several equations correlating the average grain diameter with the former parameters.
436 Accordingly, at equilibrium conditions λ and η are independent from the flow. As an example, for
437 0.1 mm sand, equilibrium λ, and η are 109 mm and 14 mm respectively (Raudkivi 1997).
438 Moreover, if the velocity u<40 cm/s and d_{50}<0.1 mm, bed morphology should be mainly
439 characterized by ripples.

Figure 7a-d shows the longitudinal profiles along sewer centreline (y=0 m), and relative to test DA-S5, AE-S6, AE-S7, AE-S8 respectively. The figure also shows the same longitudinal profiles filtered using a Gaussian filter of σ=50 mm of variance. It is possible to distinguish the formation of a long dune having large amplitude, and characterized by the superimposition of ripples. The dune is characterized by a steep leading edge (-7000 mm<x<-5500 mm), followed by a milder slope (-5500 mm<x<-2200 mm) and again by a steep part on the downstream side (-8000 mm<x<-7000 mm and -2200 mm<x<-1500 mm). On the contrary, AE longitudinal profiles are characterized by long dunes having smaller amplitudes, and shorter bed forms superimposed. For the latter, the upstream portions are generally steeper than the downstream ones. This particular pattern contrasts what generally occurs in the presence of sand dunes, and unidirectional flows, where a mild upstream slope is present which is the followed by a steeper side (Wren and Kuhnle 2008). This difference might be linked to the flow hydrograph typically observed in sewer networks, characterized by relatively low velocities and regular flow fluctuation during dry period and higher velocity during rain periods (i.e. flushing, with a steep rising limb and a relatively milder receding limb). (Campisano et al. 2004) observed similar morphologies in presence of flushing waves over isolated sediment deposits, and (Ristenpart 1995) described similar sediment morphologies with height of 5-20 cm along sewer trunk of 1500 mm of diameter.

Further insight and comparison of bed morphology can be made using Fast Fourier Analysis (FFA). Fast Fourier analysis has been successfully used by (Catano-Lopera and Garcia 2006a; Catano-Lopera and Garcia 2006b; Smith and Sleath 2005) to characterize the bed morphology for both oscillatory and combined flows. This technique allows understanding the largest component of the profile that can be assimilated to a sinusoid. Accordingly, the bottom profile can be considered as the sum of the sinusoid of wave length λ and amplitude η/2, both in mm.

The bed morphology can be approximated using a discrete sum of sinusoids:

$$z_{\mathrm{BED}}(\lambda) = \sum_{N} z_n e^{-i2\pi(\lambda/N)n} \tag{3}$$

where N is the number of simples, y_n is the n-th Fourier coefficient and:

$$\eta/2 = \left|z_{\mathrm{BED}}(\lambda)\right|/N \tag{4}$$

Figure 8 shows the fast Fourier transform (FFT) for the longitudinal profiles shown in Figure 7. The test at DA is characterised by longer amplitudes of around 7 m of wavelength, and maximum amplitude of 25 mm, while the AE test are characterised by slightly lower amplitudes of shorter wavelength, around 3.5 m. Moreover, the in case of DA test the peak can be well distinguished from the shorter wavelengths, while in case of AE the bottom centreline profile the largest harmonics is slightly larger compared to that of smaller wavelengths, most likely due to the presence of the mud layer observed in AE tests. AE tests slightly differ one each other depending on flow conditions and water depth observed during the survey. Test AE-S7 and AE-S8 shows similar peak wavelength and height of λ= 4291 mm and λ= 3362 mm and $\eta/2$= 8.5 mm and $\eta/2$= 9.2 mm respectively, although velocities and sediment height differ significantly. In contrast, test AE-S6 presented two distinct main patterns of λ= 1663 mm and λ= 3239 mm and $\eta/2$= 15.6 mm and $\eta/2$ = 17 mm respectively, that may suggest the presence of two different morphologies formed at different time. Dry days before the surveys seem to play a secondary role on the morphology, as the lowest values $\eta/2$ is observed for test AE-S8, i.e., 4 dry days from the last significant event. However, the shape and intensity of the hydrograph prior to the survey should be further analysed to better assess its role on the formation of the mud layer.

CONCLUSION

A new application of acoustic techniques to the study of morphologies, and sediment deposits in combined sewer networks has been presented. Understanding the morphological features, bed forms, and sediment characteristics of these network systems is essential as the latter highly affect the flow field, sanitation performance, as well as the risk of urban flooding.

490 The use of Sonars to investigate the morphology of sediment deposits in sewer networks has been
491 relatively unexplored but presents several advantages with respect to previous techniques, in terms
492 of both accuracy, and ease of execution. Specifically, several difficulties are associated to the use of
493 optical instruments in sewer networks due to the high suspended sediment concentrations, and
494 problems connected to the perturbation of sediment deposits when deploying the instruments. On
495 the other hand, gauge measurements can be highly subject to human errors, and are labour
496 consuming. The automated technique, and deployment presented in this paper doesn't cause any
497 perturbation of the sediment deposits, and also allowed a relatively fast reconstruction of the
498 morphology. Furthermore, a new algorithm is proposed which is aimed at identifying the sediment
499 interface by using the maximum of the gradient (rather than just the maximum) of the amplitude
500 counts. The new algorithm performs well (Figure 3b, 4), and has been applied at different sites.
501 All tests were conducted in the absence of precipitation, and after at least two days of dry weather
502 (<0.2 mm precipitation) apart from one test conducted the day after it rained. Analysing the
503 influence of rainfall events (e.g. intensity and frequency) on the sediment deposit is outside from
504 the scope of this work but is a very important aspect and deserves further investigations. In fact,
505 rainfall events influence sediment deposits and flow conditions by removing the sediment stack and
506 causing its subsequent renewal, and by influencing the bio-physicochemical conditions in the sewer
507 (e.g. Bersinger et al., 2015). Consequently, rainfall events might affect sediment reactivity, and
508 biological processes (e.g. Bersinger et al., 2015; Hannouche et al., 2014). For example, it has been
509 shown trough laboratory experiments that sediment deposits formed under flow conditions are
510 more resistant than the ones formed under quiescent water (e.g. Lau and Droppo, 2000). Bio-
511 processes are also relevant in determining the weakening or hardening of the sediment deposits. As
512 an example, nutrient depletion or high carbon to nitrogen ratio have been found to promote the
513 secretion of polymeric substances which might help the development of an organic biofilm on the
514 top of the loose sediment, and thus increase the shear threshold for erosion. In case of high oxygen
515 levels, when aerobic sediment are dominant the exopolymeric production becomes small, and an

516 intensive production of CO_2 bubbles counteracts stabilizing processes. On the other hand, when the
517 oxygen levels drops, exoploymeric production increases, and anaerobic metabolisms are favoured.
518 The latter have a weakening effect on the sediment strength due to biodegradation, and production
519 of substances such as methane which can form gas bubbles, and disturb the natural structure of the
520 sediment deposit (Baniasak et al., 2005). Further studies might address the monitoring of sediment
521 deposits characteristics and biological reactivity using acoustic measurements. For example,
522 acoustic backscatter has been related to sediment density, grain size, and sediment porosity, which
523 might be useful indicators for the biological state of the stack of deposits (Richardson and Briggs,
524 1993). Monitoring changes in such variables might also be useful to monitor the reactivity of the
525 deposit when combined with measurements of oxygen, and nutrient levels within the sewer."
526 The basic morphological features of sediment deposits have been presented for different trunks, and
527 for two field locations characterized by large differences in suspended sediment concentrations, and
528 sediment composition. Results showed that for the site with reduced suspended sediment
529 concentrations, and more non-cohesive deposits, the bed mostly displays 2D features, while in the
530 presence of a mud layer more three-dimensional patterns are present. In spite of small grain
531 diameter, the analysis of deposits centreline shows the formation of large dunes, over which smaller
532 feature superimpose. The hydraulic regime that occurs in the sewer network and the organic nature
533 of the sediment might have strongly affected dunes features which differ from those observed for
534 sandy deposits and unidirectional flow.
535

536 **AKNOWLEDGMENT**

537 The present project has been funded by the French CARNOT VITRES Institute, financial grant N°
538 07 CARN 013 01.The author would like to thank the technical staff of both the IFSTTAR (French
539 institute of science and technology for transport, development and networks) and the Nantes
540 Metropolitan Wastewater Authority for their valuable contributions to these experiments.
541

542 **REFERENCES**

543

544 Ahyerre M., Chebbo G. and Saad M. 2001, Nature and dynamics of water sediment interface in
545 combined sewers, Journal of Environmental Engineering-Asce, Vol. 127, No. 3, pp. 233-
546 239.

547 Ahyerre, M., Oms, C. & Chebbo, G. 2001 The erosion of organic solids in combined sewers. Water Science
548 and Technology 43 (5), 95-102.

549 Alexander M. P., Teeter A. M. and Banks G. E. 1997, Development and verification of an intrusive
550 hydrographic survey system for fluid mud channels, Department of the Army, U.S. Army
551 Corps of Engineers, Washington, DC.

552 Arthur S., Ashley R. M. and Nalluri C. 1996, Near bed solids transport in sewers, Water Science
553 and Technology, Vol. 33, No. 9, pp. 69-76.

554 Ashley R. M., Bertrand-Krajewski R. M., Hvitved-Jacobsen T. and Verbanck M. 2004, Solids in
555 Sewers, IWA Publishing, London, UK.

556 Ashley R. M., Wotherspoon D. J. J., Goghlen B. P. and McGregor J. 1992, The erosion and
557 movement of sediments and associated pollutants in combined sewers, Water Science and
558 Technology, Vol. 25, No. 8, pp. 101-114.

559 Aumond, M. and Joannis, C., 2008, August. Processing sewage turbidity and conductivity recorded
560 in sewage for assessing sanitary water and infiltration/inflow discharges. In *Proceedings of*
561 *the 11th International Conference on Urban Drainage, Edinburgh, Scotland, UK* (Vol. 31).

562 Banasiak, R., Verhoevena, R., De Suttera, R. & Tait, S. 2005 The erosion behavior of biologically active
563 sewer sediment deposits: observations from a laboratory study. Water Research 39, 5221-5231.
564 Bell P. S. and Thorne P. D. 1997, Application of a high resolution acoustic scanning system
565 for imaging sea bed microtopography, 7th International conference on electronic
566 engineering in oceanography, Southampton, UK, 128-133.

567 Bersinger, T., Le Hécho, I., Bareille, G., & Pigot, T. 2015 Assessement of erosion and sedimentation
568 dynamic in a combined sewer network using online turbidity monitoring. Water Science and
569 Technology 72 (8), 1375-1382.
570 Bertrand-Krajewski J.-L. and Gibello C. 2008, A new technique to measure cross-section
571 and longitudinal sediment profiles in sewers, Â Proceedings of the 11th International
572 Conference on Urban Drainage, Edinburgh, UK, 31 Aug.-5 Sept.
573 Campisano A., Creaco E. and C. M. 2004, Experimental and numerical analysis of the scouring
574 effects of flushing waves on sediment deposits Journal of Hydrology, Vol. 299, No., pp.
575 324-334.
576 Catano-Lopera Y. A. and Garcia M. H. 2006a, Geometry and migration characteristics of bedforms
577 under waves and currents - Part 2: Ripples superimposed on sandwaves, Coastal
578 Engineering, Vol. 53, No. 9, pp. 781-792.
579 Catano-Lopera Y. A. and Garcia M. H. 2006b, Geometry and migration characteristics of bedforms
580 under waves and currents. Part 1: Sandwave morphodynamics, Coastal Engineering, Vol.
581 53, No. 9, pp. 767-780.
582 Crabtree R. W. 1989, SEDIMENTS IN SEWERS, Journal of the Institution of Water and
583 Environmental Management, Vol. 3, No. 6, pp. 569-578.
584 Dolphin T. and Vincent C. 2009, The influence of bed forms on reference concentration and
585 suspension under waves and currents, Continental Shelf Research, Vol. 29, No. 2, pp. 424-
586 432.
587 El Kheiashy K., McCorquodale J., Georgiou I. and Meselhe E. 2000, Three dimensional
588 hydrodynamic modeling over bed forms in open channels, International Journal of Sediment
589 Research, Vol. 25, No. 4, pp. 431-440.
590 Gallagher E. L., Boyd W., Elgar S., Guza R. T. and Woodward B. 1996, Performance of a sonar
591 altimeter in the nearshore, Marine Geology, Vol. 133, No. 3-4, pp. 241-248.

592 Gasperi, J., Gromaire, M.-C., Kafi, M., Moilleron, R. & Chebbo, G. 2010 Contributions of wastewater,
593 runoff and sewer deposit erosion to wet weather pollutant loads in combined sewer ystems. Water
594 Research 44, 5875-5886.
595 Gourmelen L., Cottineau L.-M. and Larrarte F. 2010, Development of a system for continuos
596 sediment heigth measurements Civil and coastal engineerig workshop, Les Sables
597 d'Olonnes, France, 477-484.
598 Green M. O. and Black K. P. 1999, Suspended-sediment reference concentration under waves: field
599 observations and critical analysis of two predictive models, Coastal Engineering, Vol. 38,
600 No. 3, pp. 115-141.
601 * Hannouche, A., Chebbo, G. & Joannis, C. 2014 Assessment of the contribution of sewer deposits to
602 suspended solids loads in combined sewer systems during rain events. Environmental Science and
603 Pollution Research 21 (8), 5311-5317.
604 Hoitink A. J. F. and Hoekstra P. 2005, Observations of suspended sediment from ADCP
605 and OBS measurements in a mud-dominated environment, Coastal Engineering, Vol. 52,
606 No. 2, pp. 103-118.
607 Jaumouillie P., Larrarte F. and Milisic V. 2002, Numerical and experimental investigations of the
608 pollutant distribution in sewers, Water Science and Technology, Vol. 45, No. 7, pp. 83-93.
609 Laplace, D., Omc, C., Ahyerre, M., Chebbo, G., Lemasson, J. & Felouzis, L. 2003 Removal of the
610 organic surface layer in combined sewer sediment using a flushing gate. Water Science and
611 Technology 47 (4), 19-26.
612 Laplace D., Sanchez Y., Dartus D. and Bachoc A. 1990, SEDIMENT MOVEMENT INTO
613 THE COMBINED TRUNK SEWER NO 13 IN MARSEILLES, Water Science and
614 Technology, Vol. 22, No. 10-11, pp. 259-266.
615 Larrarte F. 2006, Velocity fields within sewers: An experimental study, Flow Measurement and
616 Instrumentation, Vol. 17, No. 5, pp. 282-290.

617 Larrarte F. 2008, Suspended solids within sewers: an experimental study, Environmental Fluid
618 Mechanics, Vol. 8, No. 3, pp. 249-261.
619 Larrarte, F. and Cottineau, L.M., 2008. The Hydre project: 2D sampling of velocities and
620 concentrations in sewer channels. *Bulletin des Laboratoires des Ponts et Chaussées*, *272*,
621 pp.21-32.
622 Larrarte, F. and Pons, M.N., 2011. Suspended solids concentration in wastewater: Influence of
623 sampling conditions. *Urban Water Journal*, *8*(6), pp.397-404.
624
625 Larrarte, F., 2015. Velocity and suspended solids distributions in an oval-shaped channel with a
626 side bank. *Urban Water Journal*, *12*(2), pp.165-173.
627 Lau, Y.L., Droppo, I.G., 2000. Influence of antecedent conditions on critical shear stress of bed
628 sediments. Water Res. 34 (2), 663–667.
629 Lee G. H., Dade W. B., Friedrichs C. T. and Vincent C. E. 2004, Examination of reference
630 concentration under waves and currents on the inner shelf, Journal of Geophysical
631 Research-Oceans, Vol. 109, No. C2.
632 Lewis C. F. M., Mayer L. A., Mukhopadhyay P. K., Kruge M. A., Coakley J. P. and Smith M. D.
633 2000, Multibeam sonar backscatter lineaments and anthropogenic organic components in
634 lacustrine silty clay, evidence of shipping in western Lake Ontario, International Journal of
635 Coal Geology, Vol. 43, No. 1-4, pp. 307-324.
636 McAnally W. H., Friedrichs C., Hamilton D., Hayter E., Shrestha P., Rodriguez H., Sheremet A.,
637 Teeter A. and Flu A. T. C. M. 2007a, Management of fluid mud in estuaries, bays, and
638 lakes. I: Present state of understanding on character and behavior, Journal of Hydraulic
639 Engineering-Asce, Vol. 133, No. 1, pp. 9-22.
640 McAnally W. H., Teeter A., Schoellhamer D., Friedrichs C., Hamilton D., Hayter E., Shrestha P.,
641 Rodriguez H., Sheremet A., Kirby R. and Fl A. T. C. M. 2007b, Management of fluid mud
642 in estuaries, bays, and lakes. II: Measurement, modeling, and management, Journal of
643 Hydraulic Engineering-Asce, Vol. 133, No. 1, pp. 23-38.

644 Menold P. H., Pearson R. K. and Allgower F. 1999, Online outlier detection and removal,
645 Proceedings of the 7th Mediterranean Conference on Control and Automation (MED99),
646 Haifa, Israel, 1110-1133.
647 Oms C. 2003, Localization, nature and dynamic of the water-sediment interface in combined sewer
648 network (in French), Ecole Nationale des Ponts et Chauséees, Paris, France.
649 Oms, C., Gromaire, M. C. & Chebbo, G. 2005 Nature and dynamic behaviour of organic surface layer
650 deposits during dry weather. Water Science and Technology 52 (3), 103-110.
651 Raudkivi A. J. 1997, Ripples on stream bed, Journal of Hydraulic Engineering-Asce, Vol. 123, No.
652 1, pp. 58-64.
653 Raudkivi A. J. 2006, Transition from Ripples to Dunes, Journal of Hydraulic Engineering, Vol.
654 132, No. 12, pp. 1316-1320.
655 Rauen W. B., Lin B. L. and Falconer R. A. 2008, Transition from wavelets to ripples in a
656 laboratory flume with a diverging channel, International Journal of Sediment Research, Vol.
657 23, No. 1, pp. 1-12.
658 Richardson, M.D. and Briggs, K.B., 1993. *On the use of acoustic impedance values to determine*
659 *sediment properties* (No. NRL/PP/7431-92-0001). NAVAL RESEARCH LAB STENNIS
660 SPACE CENTER MS.
661 Ristenpart E. 1995, Sediment Properties and their changes in a sewer, Water Science and
662 Technology, Vol. 31, No. 7, pp. 77-83.
663 Smith D. and Sleath J. F. A. 2005, Transient ripples in oscillatory flows, Continental Shelf
664 Research, Vol. 25, No. 4, pp. 485-501.
665 Thorne P. D. and Hanes D. M. 2002, A review of acoustic measurement of small-scale sediment
666 processes, Continental Shelf Research, Vol. 22, No. 4, pp. 603-632.
667 Webb M. P. and Vincent C. E. 1999, Comparison of time-averaged acoustic backscatter
668 concentration profile measurements with existing predictive models, Marine Geology, Vol.
669 162, No. 1, pp. 71-90.

Wren D. G. and Kuhnle R. A. 2008, Measurements of coupled fluid and sediment motion over mobile sand dunes in a laboratory flume, International Journal of Sediment Research, Vol. 23, No. 4, pp. 329-337.

LIST OF FIGURES

Figure 1 Sewer sketch with notation (a) Allée de l'Erdre (AE) and, (b) Duchesse Anne (DA) (dimensions in meters), looking upstream, (c) rotating head SONAR diagram sketch.
Experimental in situ set-up: (d) AE, SONAR in transverse position (submerged, flow from left) and, (e) DA, SONAR during a longitudinal survey (submerged, flow from the top of the image).
(f) Example of sediment deposit surveyed with a clear Perspex cylinder of 7 cm of internal diameter AE-S8.

Figure 2 Sonar output from laboratory experiences and in-situ conditions : (a) SONAR output in laboratory condition using AREA1 detection algorithm (white line on the image), (b) Example of in situ condition with soft sediment at the AE site (test AE-S9 x=-9.9 m); note that it is possible to detect the side bank underneath thin soft sediment deposit. Black dashed line indicates the sediment interface as identified by the program algorithm (c) Raw signal (amplitude in counts), filtered signal and gradient (counts/mm) for section y=0 m corresponding to θ=180° and j=200. The sediment interface identified by the original SONAR algorithm (peaks in counts) and by the new algorithm (peak in filtered counts gradient) are indicated as well.

Figure 3 Sonar output before and after application of the filter: (a) sonar output before filtration (test AE-S9 x=-9.9 m), (b) sonar output after filtration (test AE-S9 x=-9.9 m), the white solid circles represent the interface detected by the new algorithm. The black line below the white dots represents the interface detected with the old method. (c) Zoomed view of the sediment-water

696 interface detected with the old (black line), and new method (white dots). Note: In the figure, the
697 number of detected points (white dots) has been reduced to improve the readability; the actual
698 algorithm detects the interface with 0.9° resolution. (d) AE-S6 bottom morphology after filter
699 application.
700
701 **Figure 4** Test DA- S1 output; (a) the contour lines represent the 8 bit signal amplitude observed by
702 the sonar, (●) gauge position; pulse length of 4 μs, x=0 m, (b) 8 bit signal amplitude at y=0 cm,
703 section x=0.
704
705 **Figure 5** (a), (b), (c), (d): total suspended solid concentration, and volatile suspended solid
706 concentration (horizontal axis), free surface (vertical axis); (e), (f), (g), (h): ratio between volatile
707 suspended solids (VSS) and total suspended solids (TSS). (a), and (e) test DA-S5; (b) and (f) test
708 DA-S4; (c) and (g) test AE-S4; (d) and (h) test AE-S8. Standard deviation values for both VSS, and
709 TSS are less than 10 mg/l.
710
711 **Figure 6** Bottom morphology measured by the sonar profiler, z_{plane} in [mm] (a) DA-S5 (b) AE-S6,
712 (c) AE-S7, (d) AE-S8.
713
714 **Figure 8** longitudinal profile for y=0 m: (a) DA-S5, (b) AE-S6, (c) AE-S7, (d) AE-S8.
715
716 **Figure 9** FFT of the centreline profile.
717
718 **LIST OF TABLES**
719 **Table 1**. Flow velocity recorded before the morphological survey at the section x=0 m.
720 "site-ID" indicates the site of the measurement (DA, or AE) as well as different locations (S); Time
721 is the hour when measurements were collected; T_D is the number of dry days before the survey (i.e.,

722 less than 0.2 mm of precipitation); T is the temperature at the moment of the survey; z_{probe} indicates
723 the position of the acoustic velocity probe relative to the free surface, h is the distance from the
724 probe to the sediment interface, u is the longitudinal velocity, z_{SED} is the position of the sediment
725 detected by the point gage from the invert, δ is the total water depth between the sediment bottom
726 and the free surface.
727
728 **Table 2**. Average sediment thickness, longitudinal and transversal slopes.
729
730 NOTATION
731 a_s = diameter of the particles;
732 C = sediment concentration;
733 c = sound speed;
734 d_{xx} = diameter for which xx percent of sediment in weight is smaller;
735 h = distance from the probe to the sediment interface;
736 k = acoustic wave number;
737 $P_{L=}$ pulse length;
738 R is the distance of the generic acoustic beam from the sonar centre;
739 R_{MAX} = maximum distance that can be detected by the SONAR;
740 S= slope;
741 S_v= scattered signal in decibel;
742 S_v= scattered signal in decibel;
743 u = longitudinal velocity;
744 x,y, and z = longitudinal, transverse and vertical coordinates;
745 y_{SONAR} = transverse distance from the centre of the instrument;
746 $z_{average}$ = average surface trough the sediment bed;
747 z_{BED} = position of the sediments interface detected by the SONAR;

748 z_{plane} = sediment surface referenced from $z_{average}$;

749 z_{PROBE} = position of the velocity probe;

750 z_{SED} = position of the sediment detected by the point gage from the invert;

751 z_{SONAR} = vertical distance from the centre of the instrument;

752 α, β, and y= interpolation coefficients;

753 δ= total water depth between the sediment bottom and the free surface;

754 δ_v = vertical resolution;

755 η =wave height;

756 θ = angle between z_{SONAR} and the measured beam;

757 λ = wave length;

758 ρ_b = sediment bulk density

759 σ = standard deviation of the Gaussian filter and;

760 $\sigma_s=(d_{84}/d_{16})^{0.5}$ = uniformity parameter.

761

Table_1
Click here to download Table: Table 1.doc

Table 1 Flow velocity recorded before the morphological survey at the section x=0 m

Date	Site-ID	Time	z_{probe}	h	u	σ_u	z_{SED}	δ	T_D.	T
-	-	hours	m	m	m/s	m/s	m	m	days	°C
20-10-2010	DA-S1	8:00	-	-	0.35*	-	0.1	041	8	22
11-05-2011	DA-S5	8.00	0.1	0.34	0.41	-	0.02	0.44	2	20
11-05-2011	DA-S5	8.00	0.25	0.19	0.46	-	0.02	0.44	2	20
25-11-2010	AE-S2	8:00	-	-	0.10*	-	0.2	0.93	0	19
10-03-2011	AE-S6	7.50	0.1	0.37	0.116	0.026	0.35	0.47	10	15.6
10-03-2011	AE-S6	7.50	0.2	0.27	0.086	0.003	0.35	0.47	10	15.6
24-03-2011	AE-S7	10.18	0.5	0.11	0.0695	0.015	0.12	0.61	7	16
24-03-2011	AE-S7	10.19	0.4	0.21	0.1085	0.004	0.12	0.61	7	16
24-03-2011	AE-S7	10.19	0.3	0.31	0.1285	0.006	0.12	0.61	7	16
24-03-2011	AE-S7	10.21	0.2	0.41	0.1355	0.008	0.12	0.61	7	16
24-03-2011	AE-S7	10.21	0.1	0.51	0.1445	0.004	0.12	0.61	7	16
04-05-2011	AE-S8	10.18	0.2	0.21	0.097	0.004	0.35	0.41	4	19
04-05-2011	AE-S8	10.19	0.3	0.11	0.085	-	0.35	0.61	4	19

* average velocity from discharge measurements

Table 2. *Average* sediment thickness, longitudinal and transversal slopes.

Survey [-]	α [mm]	β [-]	γ [-]
DA-S5	16	-0.002	-0.072
AE-S6	302	-0.035	-0.081
AE-S7	297	-0.006	-0.014
AE-S8	355	-0.022	0.045

Figure_1

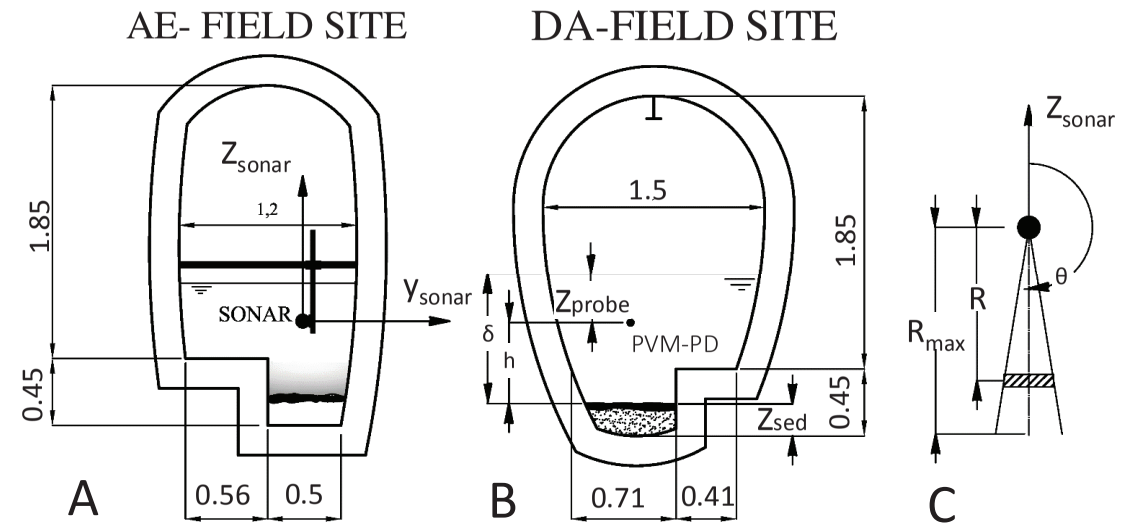
AE- FIELD SITE
DA-FIELD SITE
Z sonar
1,2
1.85
SONAR
y sonar
0.45
A
0.56
0.5
δ
h
Z probe
PVM-PD
1.5
1.85
Z sed
0.45
B
0.71
0.41
Z sonar
θ
R
R max
C

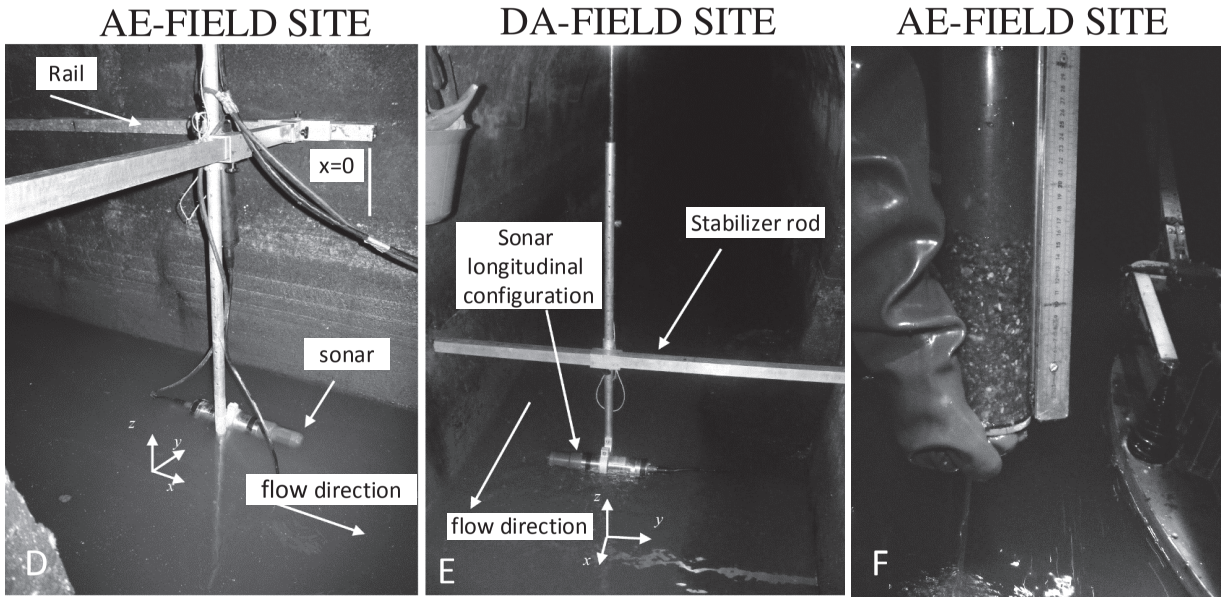
AE-FIELD SITE
DA-FIELD SITE
AE-FIELD SITE
Rail
x=0
sonar
flow direction
D
Sonar longitudinal configuration
Stabilizer rod
flow direction
E
F

Figure_2

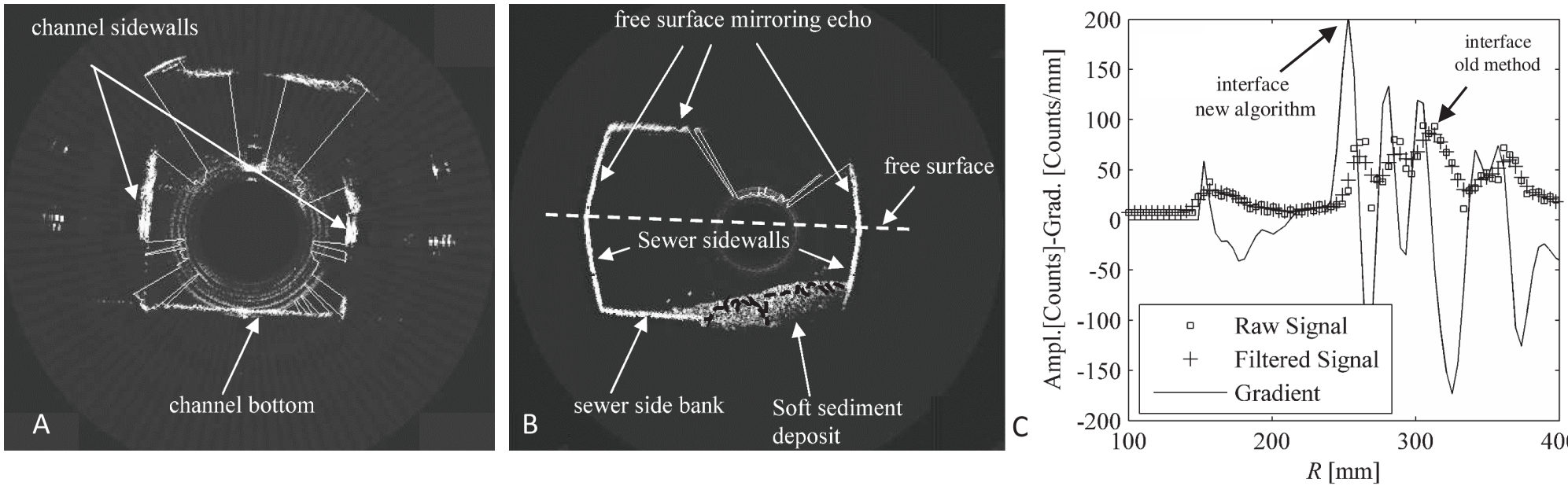
channel sidewalls
channel bottom
A
free surface mirroring echo
free surface
Sewer sidewalls
sewer side bank
Soft sediment deposit
B
C
interface new algorithm
interface old method
Raw Signal
Filtered Signal
Gradient
Ampl.[Counts]-Grad. [Counts/mm]
R [mm]
200
150
100
50
0
-50
-100
-150
-200
100
200
300
400

Figure_3

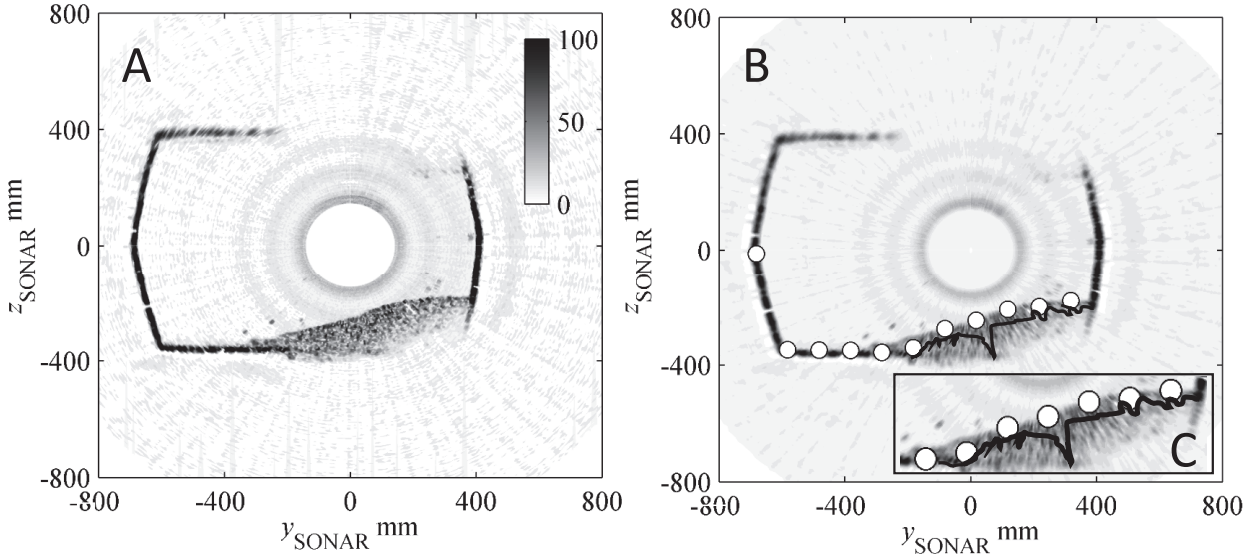
A
B
C
100
50
0
800
400
0
-400
-800
z_{SONAR} mm
y_{SONAR} mm

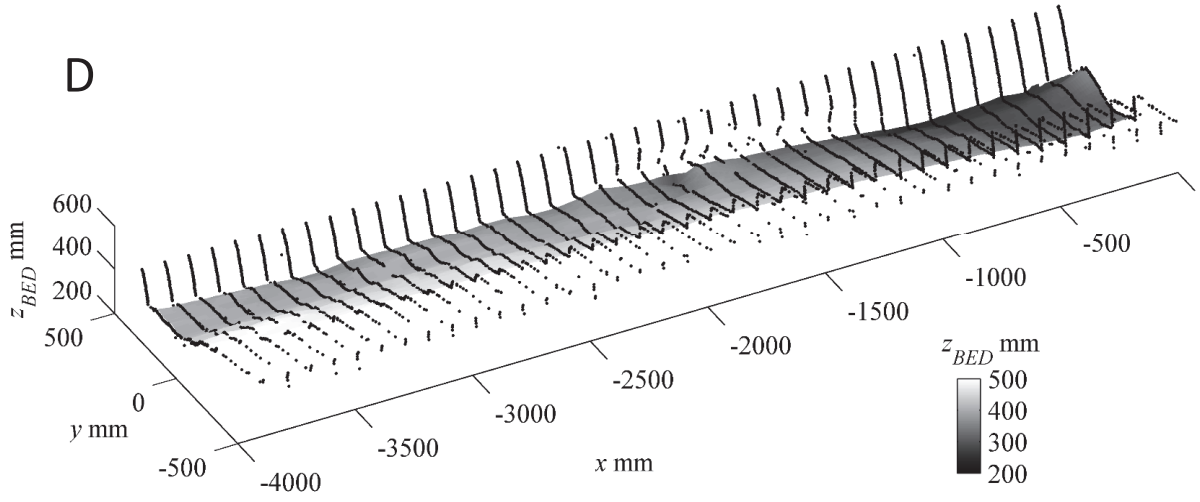
D
600
400
200
z_{BED} mm
500
0
-500
y mm
-4000
-3500
-3000
-2500
-2000
-1500
-1000
-500
x mm
z_{BED} mm
500
400
300
200

Figure_4

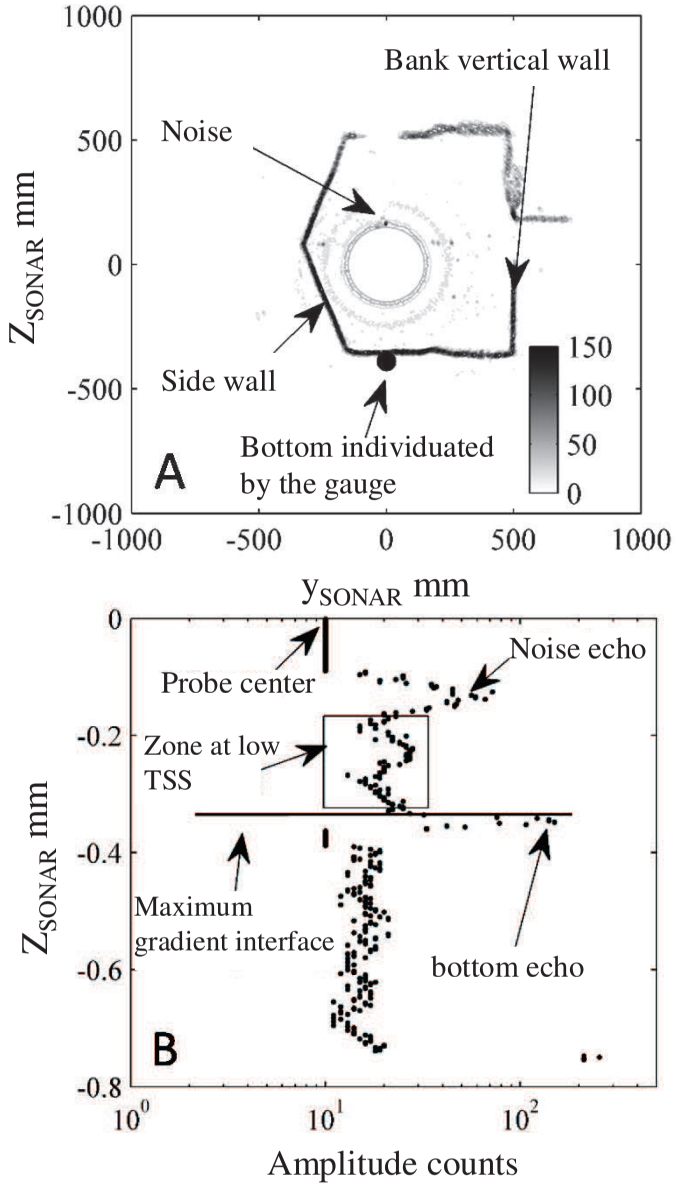
Bank vertical wall
Noise
Side wall
Bottom individuated
by the gauge
A
150
100
50
0
1000
500
0
-500
-1000
Z_{SONAR} mm
y_{SONAR} mm
Noise echo
Probe center
Zone at low
TSS
Maximum
gradient interface
bottom echo
B
-0.2
-0.4
-0.6
-0.8
10^0
10^1
10^2
Amplitude counts

Figure_5

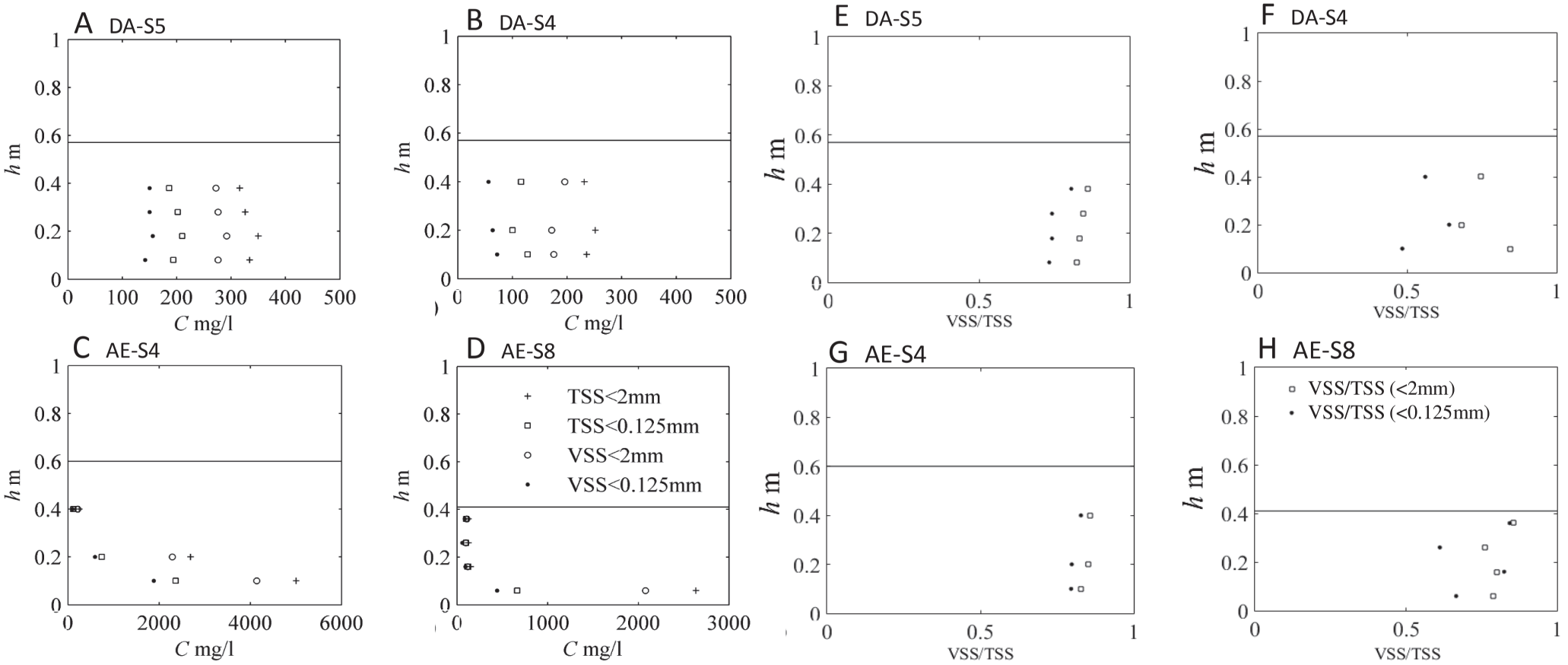
A DA-S5
B DA-S4
E DA-S5
F DA-S4
C AE-S4
D AE-S8
G AE-S4
H AE-S8
h m
C mg/l
VSS/TSS
TSS<2mm
TSS<0.125mm
VSS<2mm
VSS<0.125mm
VSS/TSS (<2mm)
VSS/TSS (<0.125mm)

Figure_6

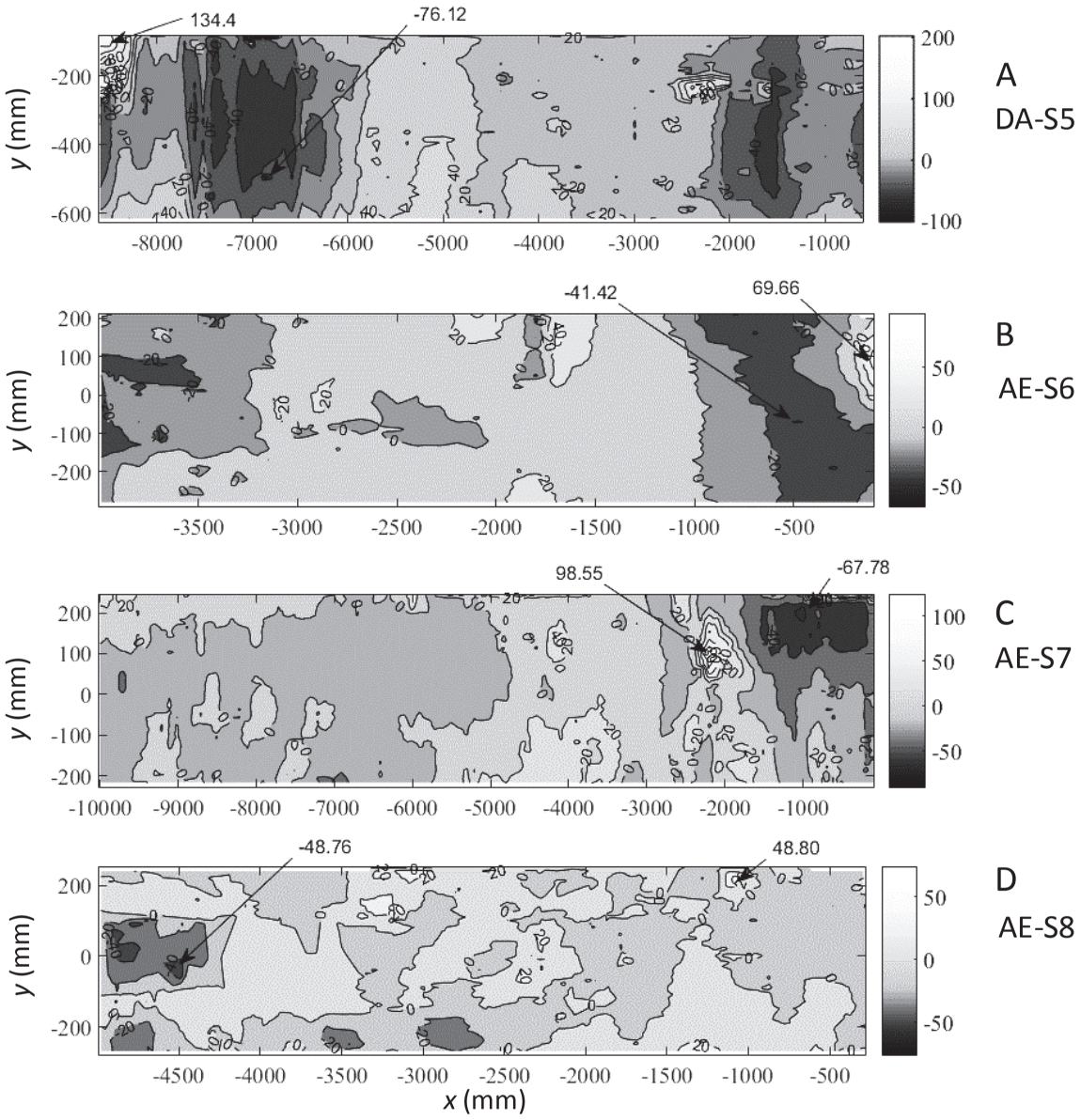
134.4
-76.12
y (mm)
-200
-400
-600
-8000
-7000
-6000
-5000
-4000
-3000
-2000
-1000
200
100
0
-100
A
DA-S5
-41.42
69.66
y (mm)
200
100
0
-100
-200
-3500
-3000
-2500
-2000
-1500
-1000
-500
50
0
-50
B
AE-S6
98.55
-67.78
y (mm)
200
100
0
-100
-200
-10000
-9000
-8000
-7000
-6000
-5000
-4000
-3000
-2000
-1000
100
50
0
-50
C
AE-S7
-48.76
48.80
y (mm)
200
0
-200
-4500
-4000
-3500
-3000
-2500
-2000
-1500
-1000
-500
x (mm)
50
0
-50
D
AE-S8

Figure_7

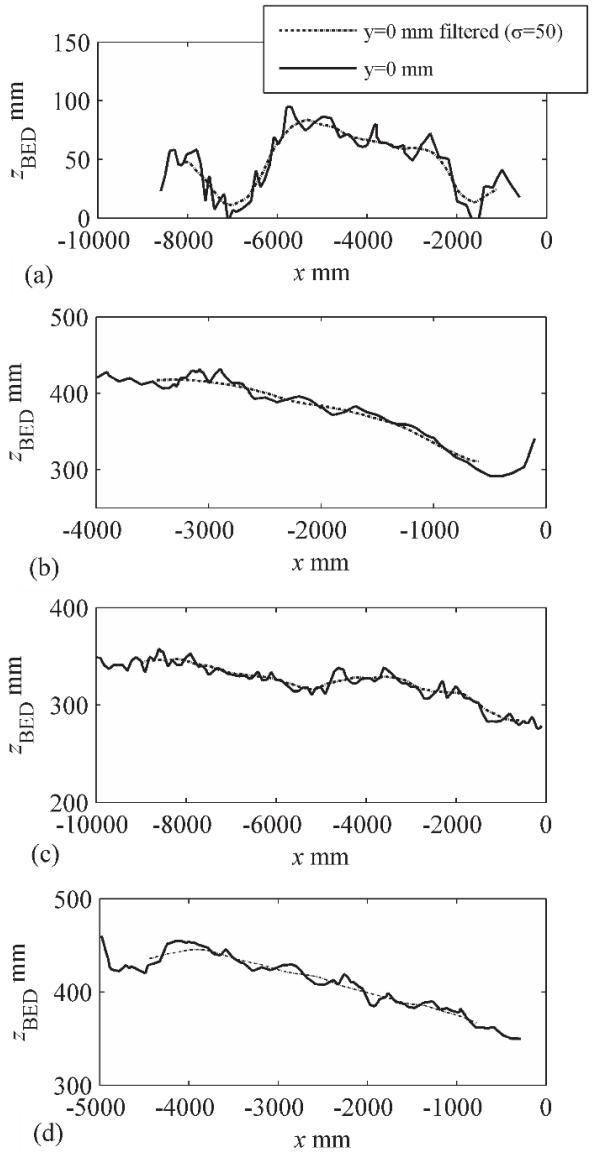
y=0 mm filtered (σ=50)
y=0 mm
150
100
50
0
z_{BED} mm
-10000 -8000 -6000 -4000 -2000 0
x mm
(a)
500
400
300
z_{BED} mm
-4000 -3000 -2000 -1000 0
x mm
(b)
400
300
200
z_{BED} mm
-10000 -8000 -6000 -4000 -2000 0
x mm
(c)
500
400
300
z_{BED} mm
-5000 -4000 -3000 -2000 -1000 0
x mm
(d)